Available online at www.sciencedirect.com
ScienceDirect
Journal of Magnetism and Magnetic Materials 320 (2008) 1412–1422
Journal of magnetism and magnetic materials
www.elsevier.com/locate/jmmm

Multiscale modeling of the magneto-mechanical behavior of grain-oriented silicon steels

O. Hubert[a,*], L. Daniel[b]

[a]LMT-Cachan, (ENS Cachan/CNRS UMR8535/UPMC/PRES UniverSud Paris) 61, avenue du Président Wilson, F-94235 CACHAN Cedex, France
[b]Laboratoire de Génie Electrique de Paris (LGEP), CNRS UMR8507; SUPELEC; UPMC Univ Paris 06; Univ Paris-Sud; 11, rue Joliot-Curie, Plateau de Moulon, F-91192 Gif-sur-Yvette cedex, France

Received 10 July 2007; received in revised form 24 November 2007
Available online 12 January 2008

Abstract

The prediction of the magnetic and magnetostrictive behavior of grain-oriented (GO) silicon steels is discussed. An experimental procedure for the measurement of the magneto-mechanical quantities is first detailed. Experimental measurements of the anhysteretic magnetization and magnetostriction are compared to results from the literature. A multiscale model, based on an energetic approach and infinite medium hypothesis, is used. Significant discrepancies between experiments and predictions are highlighted. The specimen shape combined to large grain size induces some strong boundary (surface) conditions leading to a change in the definition of the local potential energy. A specific demagnetizing term is introduced in the definition of the potential energy, creating an initial heterogeneous distribution of the magnetic domains and saturating the magnetostriction along the rolling direction. This modification strongly increases the ability of the model to predict the magneto-mechanical behavior of GO steels.

PACS: 75.60.−d; 75.80.+q; 75.30.Gw; 75.50.Bb

Keywords: Silicon–iron; Grain-oriented (GO); Experiments; Modeling; Demagnetizing surface effect; Magnetostriction

1. Introduction

The research for lower core losses and audible noise in the modern electrical machines and systems requires adequate mathematical models able to predict the complex anisotropic magnetic and magneto-mechanical behavior of industrial ferromagnetic materials in order to give help for more accurate design. These models must take into account the complex thermo-magneto-mechanical loadings (e.g. rotating magnetic field, harmonics, stress field, plastic strains, thermal field) that the material can be submitted to. Grain-oriented (GO) silicon–iron alloy is one of the most popular soft ferromagnetic materials. GO silicon–iron alloys, exhibiting the so-called GOSS texture,[1] are widely used in high power transformers because of their very good magnetic properties along the rolling direction (RD) [1,2], and literature concerning their magnetic behavior (magnetization [3]; losses [4]; modeling [5]; metallurgy [6]; effect of stress [7]; effect of plasticity [8]) and other properties (magnetostriction [9]; ΔE effect [10]) is numerous.

The laminations are usually stacked together and assembled. Such structures are on the other hand well known to emit vibrations and noise [11]. This phenomenon has two possible origins: usual magnetic forces and associated elastic deformations (that induces the so-called form effect [12]), and magnetostriction strain [13] strongly correlated to the crystallographic texture and orientation of the magnetic field with respect to the RD [11,14]. The first source depends on the geometry of the structure (global coupling) and can be obtained after finite element modeling [15,16]. The second is usually considered as material dependent (local coupling) and needs a specific constitutive equation to be evaluated [17].

*Corresponding author. Tel.: +33 1 47 40 22 24; fax: +33 1 47 40 22 40.
E-mail addresses: hubert@lmt.ens-cachan.fr (O. Hubert), laurent.daniel@lgep.supelec.fr (L. Daniel).

[1]"GOSS" stands for: Grain-Oriented Silicon Steel.

0304-8853/$ - see front matter © 2008 Elsevier B.V. All rights reserved.
doi:10.1016/j.jmmm.2008.01.013

No model can accurately predict magnetostriction strain, especially when a mechanical stress is superimposed to the magnetic loading. This phenomenon has already been observed and discussed. Our objective is to propose a model in order to give an accurate prediction of the magneto-mechanical properties (i.e. magnetic and magnetostrictive behavior) of this kind of material submitted or not to stress. This work requires to get new experimental results (especially anhysteretic) to be compared to the modeling results.

In this paper, the experimental procedure to get the magneto-mechanical behavior of a GO 3% silicon–iron alloy is first presented giving results in good accordance with previous results of the literature. A model, based on an energetic approach and transition scale rules, has been proposed to predict the complex magneto-elastic behavior of bulk ferromagnetic materials [18]. The model is a representative volume element (RVE) model independent from boundary conditions. In this paper, it is shown that a structural demagnetizing energy term is required in the definition of local energy to make the model fit properly the experimental observations for laminations (magnetic domains distribution, magnetic and magnetostrictive behavior).

2. Experimental observations

2.1. Material: description and mechanical properties

A standard industrial GO 3% silicon–iron lamination (Hi-B—0.3 mm thick from Nippon Steel) has been chosen for the study. The grain size of the material is very high reaching 40 mm (Fig. 1). An orientation data file (ODF) has been obtained from electron back-scattered diffraction (EBSD) measurements. Fig. 2 shows the resulting pole figures (surface of analysis is about 25 cm^2—which corresponds approximately to 60 points of measurements on 10 grains). A strong usual GOSS texture $\{1\,1\,0\}\langle 0\,0\,1\rangle$ is clearly highlighted (strong $\langle 1\,0\,0\rangle$ pole along RD and $\langle 1\,1\,0\rangle$ pole along TD[2]), and some disoriented grains are detected.[3]

Moreover, previous stress–strain experiments allowed us to measure the elastic properties of the material [20]. Samples consist of 250 mm long and 12.5 mm wide bands. Strain gages have been stuck on some selected grains[4] to get their mechanical behavior associated to spatial orientation. We get two terms of the elastic deformation tensor $\boldsymbol{\varepsilon}_e$ as a function of the tensile stress tensor $\boldsymbol{\sigma}$. Once the disorientations have been taken into account, the elastic stiffness tensor $\mathbb{C}^g$ of the single crystal is calculated thanks to an inverse procedure (Hooke law: $\boldsymbol{\sigma} = \mathbb{C}^g \cdot \boldsymbol{\varepsilon}_e$).

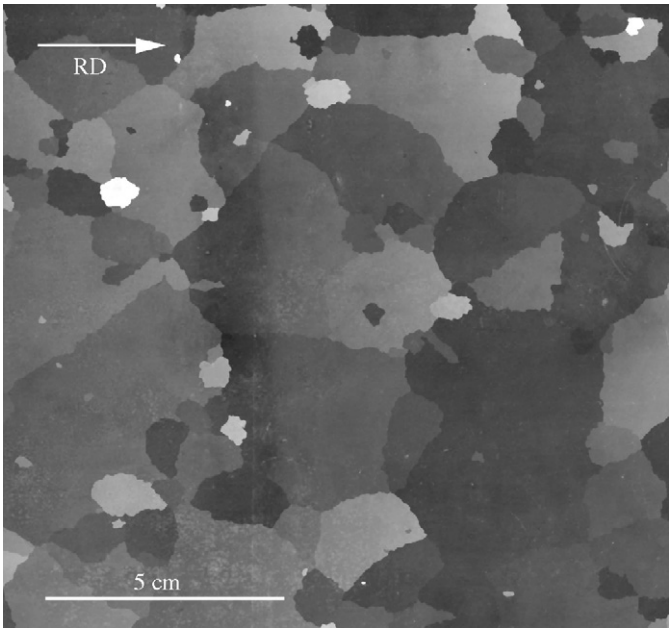

Fig. 1. Sheet after the removal of the coating (HCl–HF etching) [19].

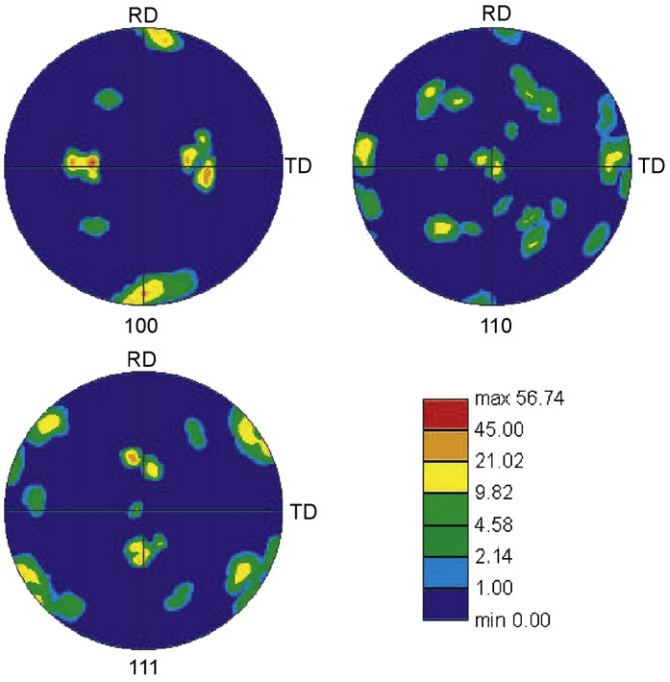

Fig. 2. Pole figures of the material (EBSD measurement—from UTC Compiégne—France).

$\mathbb{C}^g$ depends on three constants to model a cubic symmetry (C_{11}, C_{12} and C_{44} using Voigt notation) [21]. Values can be found in Table 1 later in the paper.

2.2. Magneto-mechanical measurements

An original benchmark has been employed to measure the magneto-elastic behavior (see Refs. [22,14]). Fig. 3

[2]RD is for rolling direction, TD for transverse direction.

[3]This texture is correlated to a low grade Hi-B material.

[4]The grains must be big enough to make firstly both mechanical and magnetic measurements possible, and secondly an indexation by EBSD. We verify on the other hand that the orientation of the grains we chose is representative of the orientation of the material—the area of EBSD measurement can be seen in Fig. 3.

Table 1
Physical constants used for the multiscale modeling

Coefficient	M_s	K_1 ; K_2	λ_{100} ; λ_{111}	A_s	C_{11} ; C_{12} ; C_{44}
Unit	A/m	kJ m^{-3}	–	m^3 J^{-1}	GPa
Value	1.61×10^6	38; 0	23×10^{-6} ; -4.5×10^{-6}	2×10^{-2}	202; 122; 229

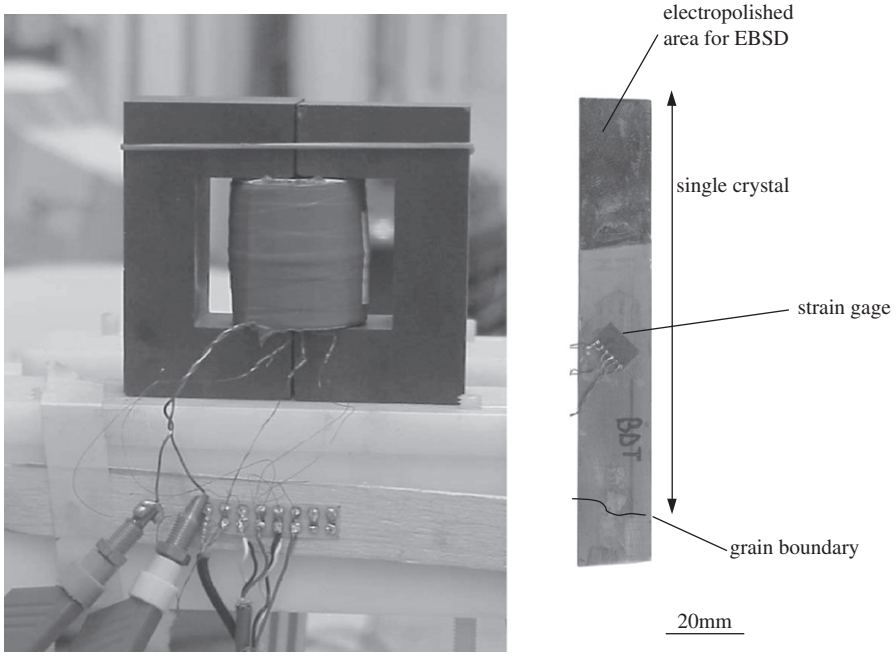

Fig. 3. Experimental set-up for magneto-mechanical measurements—instrumented sample.

shows the double U-yoke set-up and an example of sample that has been used for the study. The specimen is about 60 mm long and 12 mm wide. Only one end of the sample is pressed between the yokes (upper end in Fig. 3). The other end is let free to move (only submitted to a low friction) in order to avoid any mechanical stress, which could disturb the measurement of magnetostriction. This set-up ensures the magnetization of a single grain.[5] The specimens are magnetized thanks to a 50 turns primary coiling. The pick-up coil is directly wound around the sample. The magnetic loading is ensured by a current amplifier controlled by a self-developed Labview program [23]. Results presented hereafter are composed of hysteretic (0.1 Hz triangular current form) and anhysteretic loadings: anhysteretic curves[6] are measured point by point by applying a sinusoidal magnetic field of mean value H_{an}, and of exponentially decreasing amplitude. The magnetostriction is measured simultaneously thanks to non-magnetoresistive strain gages stuck on both sides of the sample (Fig. 3). A half Wheatstone bridge configuration with temperature compensation has been chosen for strain measurement (the signal is stored after a low-pass second order Butterworth filtering) [14]. Note that the anhysteretic procedure makes the measurement of the magnetostriction behavior more accurate, less noisy and more reproducible than a usual hysteretic measurement. The error of measurement for the deformation is estimated to $\pm 5 \times 10^{-7}$ considering gage factor fluctuations,[7] electrical noise level and observed dispersions (Fig. 4).

Remark. The measured deformation is not rigorously "pure" magnetostriction because the parasitic elastic deformation due to the magnetic forces still remains (i.e. form effect) [12,16]. This deformation is sometimes of the same order of magnitude and has the same dynamic (frequency, even function) than magnetostriction. A correction procedure should rigorously be applied.[8] Nevertheless recent finite element calculations [25] showed that

[5]Fig. 3 shows that the active part of the sample is composed of only one big grain. All experiments have been made in such condition.

[6]The anhysteretic behavior is theoretically related to the reversible behavior of the material; this measurement is to be compared to the modeling results.

[7]A deformation ε is related to relative variation of resistance of the gage $\Delta R/R$ thanks to $\varepsilon = (1/K)(\Delta R/R)$ where K is the gage factor $-K = 2.1 \pm 2\%$.

[8]A calculation of magnetic forces in a previous set-up and associated elastic deformations can be found in Ref. [22]. The formulation of magnetic forces is due to Ref. [24].

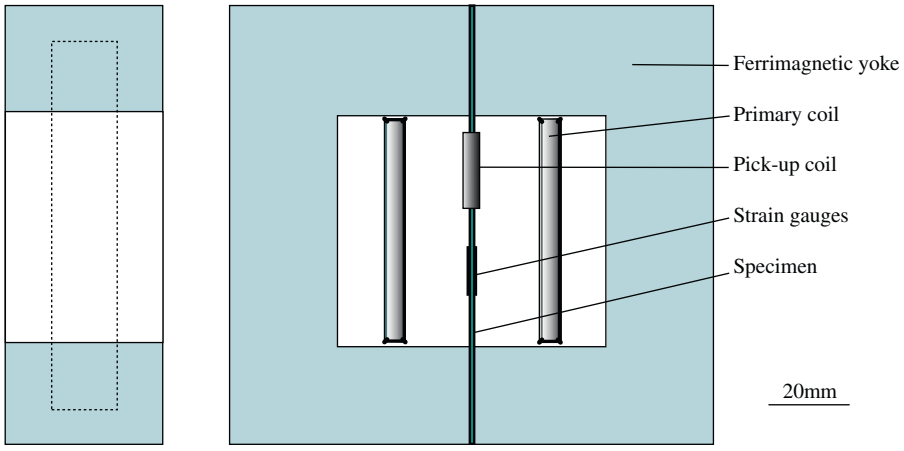

Fig. 4. Details of the experimental set-up.

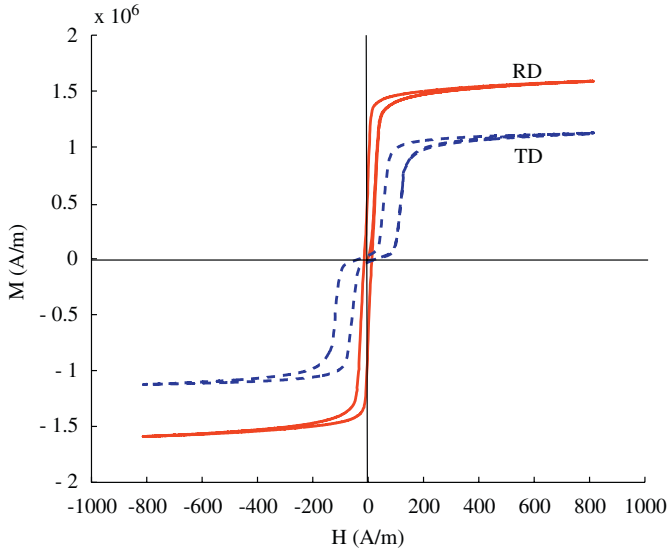

Fig. 5. Magnetization and hysteretic curves along RD and TD.

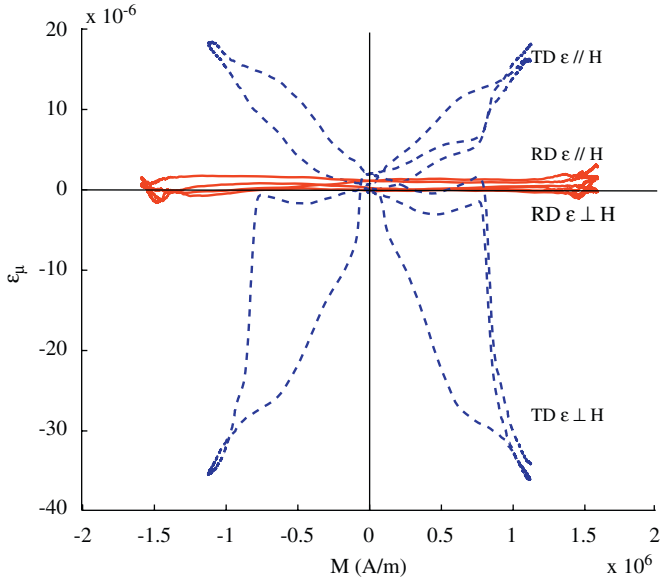

Fig. 6. Hysteretic magnetostriction curves along RD (full lines) and TD (dashed lines) associated to the loading of Fig. 5.

the form effect is negligible for this kind of structure (thin sample and flux closed by the yokes). Results presented hereafter are consequently not corrected.

Fig. 5 shows the magnetization and hysteretic curves of the material carried out at 0.1 Hz along RD and TD. These results are classical, especially the non-conventional form of the TD behavior [8,5]. Fig. 6 shows the associated hysteretic magnetostriction curves of the material. Deformation measurement has been carried out along the longitudinal (parallel to the magnetization direction) and transversal (perpendicular to the magnetization direction) directions for each magnetic loading. The deformation associated to a magnetic loading along RD is very low: it is approximately of the same order than the precision of measurement, and a cycle is consequently difficult to observe. The amplitude of deformation associated to a magnetic loading along TD is much higher, especially for the transversal gage. Deformation is reaching 2×10^{-5} along the longitudinal direction and approximately -3.5×10^{-5} at 90°. Two strongly geometrical cycles can be observed.

Fig. 7 allows us to compare the anhysteretic curves for two directions (the figure is drawn using a logarithmic format): the maximum anhysteretic susceptibility is reaching 8×10^4 for RD. Two samples per direction have been used to make this experiment. We observe some differences for the samples cut along the same direction, that is probably due to the weak disorientation of the grains which are tested. The full and dashed lines give average curves for both directions.

Experimental anhysteretic magnetostriction has been carried out with magnetization along RD and TD. Results are plotted in two figures for a better clarity: longitudinal measurements are reported in Fig. 8; transversal measurements are reported in Fig. 9. Because of the very small

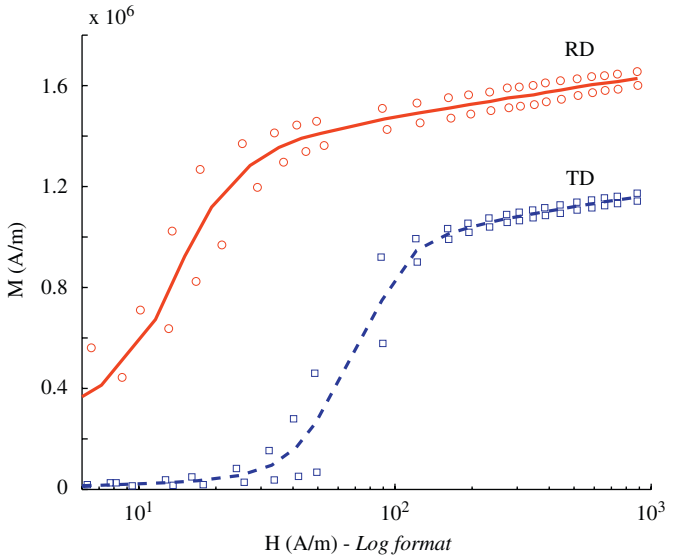

Fig. 7. Experimental measurement of the anhysteretic magnetization curves along RD (full lines) and TD (dashed lines). The points give an idea of the dispersion from a sample to another.

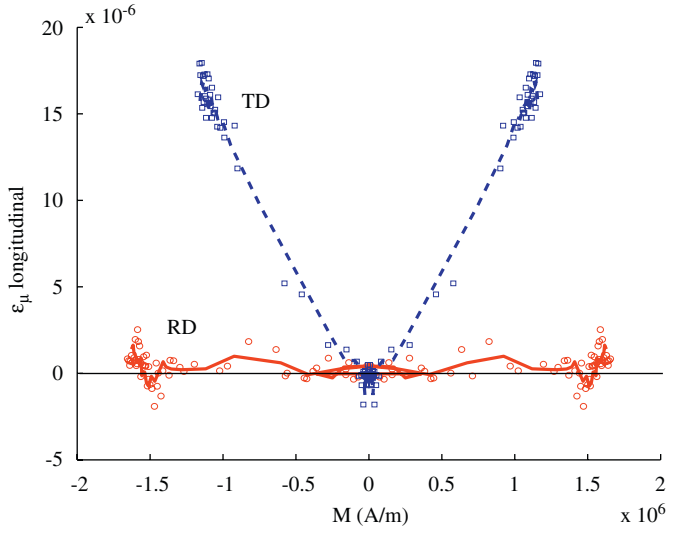

Fig. 8. Experimental measurement of the anhysteretic longitudinal magnetostriction along RD (full) and TD (dashed).

amplitude of deformation, the sensitivity of magnetostriction to stress and the high grain size, several measurements carried out on different specimens, using small strain gages ($2\,mm^2$) and a statistical treatment of the results have been required. Magnetostriction is strongly anisotropic. Amplitudes vary from approximately zero for RD to 18×10^{-6} for TD-longi and -37×10^{-6} for TD-trans.

2.3. Comparison to results from literature and discussion

A first step consists in comparing our measurements to the results published in the literature. Experimental results

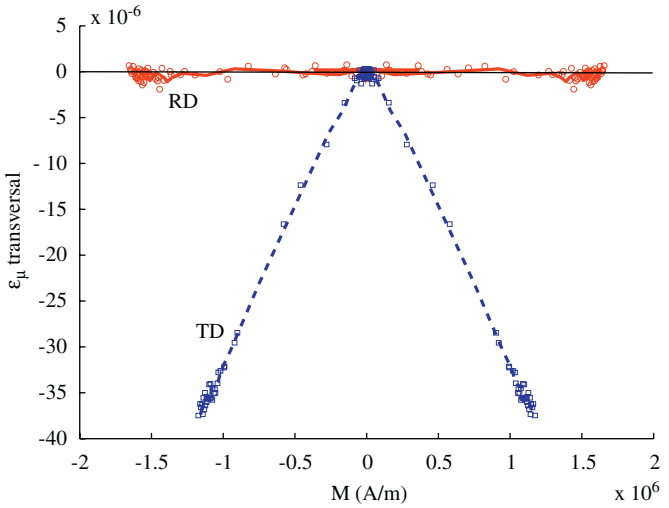

Fig. 9. Experimental measurement of the anhysteretic transverse magnetostriction along RD (full) and TD (dashed).

of Ban and Janosi [9] and Ushigami et al. [26] have been reported in Fig. 10. Our results seem noisier but tendencies are in good accordance. We observe that magnetostriction remains zero (considering the precision of measurement) until M reaches $0.9–1.1 \times 10^6\,A/m$. Magnetostriction increases for higher magnetization levels (due to a weak magnetization rotation) and saturates. The experimental saturation value is about $\lambda_{max} \approx 2 \pm 1 \times 10^{-6}$; it is reached for a magnetization up to $16 \times 10^5\,A/m$. The maximal deformation measured by other authors stays around $1–2 \times 10^{-6}$. An area defined in Ref. [2] has been added to the graph. It represents a domain of existence of the magnetostriction for a usual GO magnetized along RD. Our results are in accordance with this area and especially some negative points at high field. Few results are available in the literature concerning the magnetostrictive behavior when the magnetization is applied along TD. We can only report the observations of Sheiko et al. [27] whose results are in good accordance with ours.

A single crystal approach is chosen to discuss these results. Considering the crystallographic texture of the material, RD is corresponding to a $\langle 1\,0\,0\rangle$ direction and TD to a $\langle 1\,1\,0\rangle$ direction (cf. Fig. 11). Magnetostrictive results got on a GO lamination may consequently be in accordance with the saturation magnetostriction of a silicon–iron single crystal measured along the same crystallographic direction (e.g. λ_{100} for RD). Cullity [2] and Weiser and Pfützner [13] give for example a value of $\lambda_{100} = 23 \times 10^{-6}$ for the composition of material. The maximal magnetostriction we measured is then ten times lower than the value expected. Such a difference was already observed by Weiser and Pfützner [13] and proves that a model only based on the behavior of the single crystal is not accurate. The domain configuration must not be neglected.

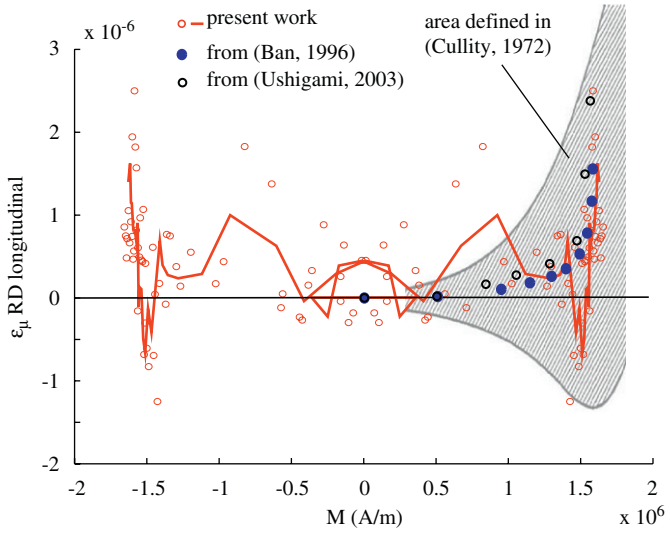

Fig. 10. Comparison to previous results from literature.

It is known that the ideal configuration of domains in one grain of a GO sheet consists in two domains α_1 and α_2 separated by one 180° wall (Fig. 11a) [28]. Eq. (1) gives the magnetostriction strain tensor in the crystallographic frame (CF) [29]. γ_i are the direction cosines of the magnetization vector in the same frame. Eq. (2) consequently defines the magnetostriction strain tensor of each domain and thus of the associated grain in CF, when no magnetic field is applied.

$$\varepsilon_{\mu}^{\alpha} = \frac{3}{2}\begin{pmatrix} \lambda_{100}\left(\gamma_1^2 - \frac{1}{3}\right) & \lambda_{111}\gamma_1\gamma_2 & \lambda_{111}\gamma_1\gamma_3 \\ \lambda_{111}\gamma_1\gamma_2 & \lambda_{100}\left(\gamma_2^2 - \frac{1}{3}\right) & \lambda_{111}\gamma_2\gamma_3 \\ \lambda_{111}\gamma_1\gamma_3 & \lambda_{111}\gamma_2\gamma_3 & \lambda_{100}\left(\gamma_3^2 - \frac{1}{3}\right) \end{pmatrix}_{CF}, \quad (1)$$

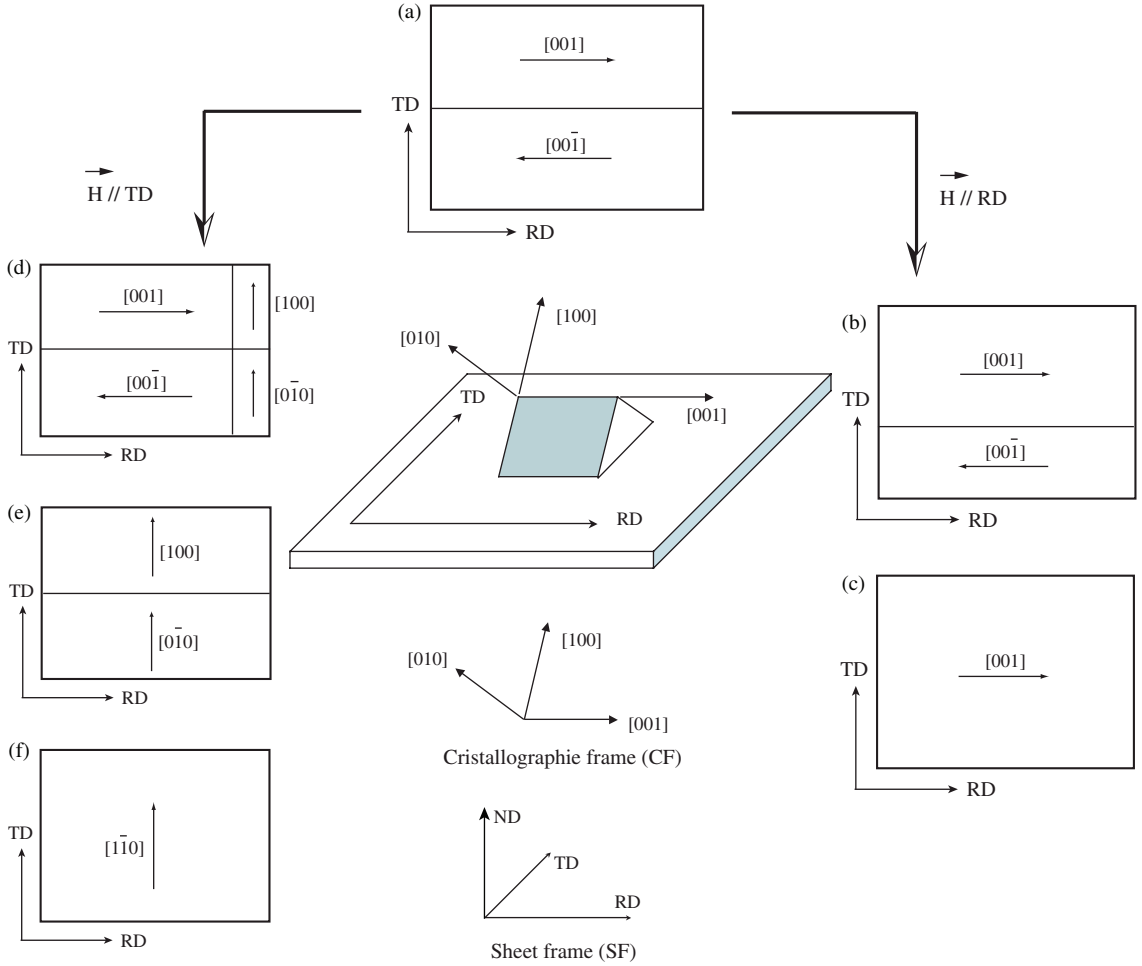

Fig. 11. Bi-domains elementary distribution in a grain (scheme) separated by a 180° domain wall: (a) ideal initial configuration; (b) low magnetization along RD—wall displacement—until magnetic saturation (c); (d) low magnetization along TD—nucleation of orthogonal domains; (e) intermediate magnetization along TD—disappearance of the initial domain structure; (f) magnetization up to saturation along TD—magnetization rotation out of the easy crystallographic axes. Definition of crystallographic and sheet frames (denoted CF and SF): ND: normal direction.

$$\boldsymbol{\varepsilon}_{\mu}^{\alpha_1} = \boldsymbol{\varepsilon}_{\mu}^{\alpha_2} = \begin{pmatrix} -\frac{1}{2}\lambda_{100} & 0 & 0 \\ 0 & -\frac{1}{2}\lambda_{100} & 0 \\ 0 & 0 & \lambda_{100} \end{pmatrix}_{\mathrm{CF}} = \boldsymbol{\varepsilon}_{\mu}^{g}. \tag{2}$$

The magnetic loading up to saturation along RD (Figs. 11b and c) leads to no change of magnetostriction along this direction ($\boldsymbol{\varepsilon}^{\mathrm{g}}_{\mu\vec{H}\|\mathrm{RD}}(M) = \boldsymbol{\varepsilon}^{\mathrm{g}}_{\mu}$). Magnetostrictive behavior along RD must consequently be theoretically zero whatever the magnetization level. In this condition, $\Delta\lambda_{\mathrm{longi}} = \Delta\lambda_{\mathrm{trans}} = 0$ when the material is magnetized along RD.[9] This interpretation is in accordance with the very low values we measured with RD specimens (see also Ref. [26]).

$$\boldsymbol{\varepsilon}'^{\mathrm{g}}_{\mu\vec{H}\|\mathrm{TD}} = \langle \boldsymbol{\varepsilon}_{\mu}^{\alpha_3} + \boldsymbol{\varepsilon}_{\mu}^{\alpha_4} \rangle = \begin{pmatrix} \frac{1}{4}\lambda_{100} & 0 & 0 \\ 0 & \frac{1}{4}\lambda_{100} & 0 \\ 0 & 0 & -\frac{1}{2}\lambda_{100} \end{pmatrix}_{\mathrm{CF}}, \tag{3}$$

$$\boldsymbol{\varepsilon}^{\mathrm{g}}_{\mu\vec{H}\|\mathrm{TD}}(M_{\mathrm{s}}) = \begin{pmatrix} \frac{1}{4}\lambda_{100} & -\frac{3}{4}\lambda_{111} & 0 \\ -\frac{3}{4}\lambda_{111} & \frac{1}{4}\lambda_{100} & 0 \\ 0 & 0 & -\frac{1}{2}\lambda_{100} \end{pmatrix}_{\mathrm{CF}}. \tag{4}$$

When the material is magnetized along TD, domain wall motion and magnetization rotation can occur simultaneously. If the magnetization rotation is considered only for high fields (high magnetocrystalline constant K_1 value—see Table 1), the first step is the nucleation of transversal domains (α_3, α_4) along the most favorable easy magnetic axes (Fig. 11d) [28]. This mechanism is continuing until the previous magnetic structure disappears (Fig. 11e). At this point, the magnetostriction tensor of the grain is given by expression (3) and we can estimate: $\Delta\lambda_{\mathrm{longi}} = (\frac{1}{4}\lambda_{100} + \frac{1}{2}\lambda_{100})$. The last step is the magnetization rotation until saturation (Fig. 11f), leading to $\gamma_1 = \gamma_2 = \cos(\pi/4) = \sqrt{2}/2$ and $\gamma_3 = 0$. The magnetostriction tensor of the grain is now given by expression (4), and thus $\Delta\lambda_{\mathrm{longi}} = (\frac{1}{4}\lambda_{100} + \frac{3}{4}\lambda_{111} + \frac{1}{2}\lambda_{100})$; the transversal measurement remains the same before and after the magnetization rotation: $\Delta\lambda_{\mathrm{trans}} = (-\frac{1}{2}\lambda_{100} - \lambda_{100})$.

Once calculated using silicon–iron constants (Table 1), we get for a magnetization along TD $\Delta\lambda_{\mathrm{longi}} = 17.25 \times 10^{-6}$ at stage corresponding to Fig. 11e, then $\Delta\lambda_{\mathrm{longi}} = 13.875 \times 10^{-6}$ at stage corresponding to Fig. 11f. The transverse magnetostriction is negative and twice higher: $\Delta\lambda_{\mathrm{trans}} = -34.5 \times 10^{-6}$. These different values can be easily put in regard to the experimental data (Figs. 8 and 9): the null value of longitudinal and transversal deformations for RD specimens is clearly observed; for TD specimens, the two stages for longitudinal deformation are verified and experimental values for the amplitudes are in very good accordance with theoretical ones; the amplitude of transversal deformation is reaching the foreseen value too.

This simple approach is seducing but insufficient because it only gives bound values but no behavior. Moreover the coupling with stress is not considered. The next paragraph is devoted to a more accurate modeling.

[9] We define $\Delta\lambda_{\vec{n}}(M) = \vec{n}^{t} \cdot (\boldsymbol{\varepsilon}^{\mathrm{g}}_{\mu}(M) - \boldsymbol{\varepsilon}^{\mathrm{g}}_{\mu}) \cdot \vec{n}$, where $\vec{n}$ is the direction of measurement.

3. Multiscale modeling

Multiscale approaches are of great interest when the phenomena are the result of anisotropies at different scales [30]: here the usual cubic anisotropy at the grain scale and the small disorientation of the grains (macroscopic texture) at a larger scale. An implicit method is employed to homogenize the magnetic, mechanical and magnetostrictive behavior [31,18]. The distribution of grains of cubic symmetry structure is considered inside a homogeneous orthotropic equivalent medium. The ODFs are issued from the previous EBSD measurement. The calculations have been implemented using mechanical and magnetic characteristics of silicon–iron single crystals.

3.1. Micromagnetic model (grain scale) [18]

GO ferromagnetic media can be considered as an aggregate of single crystals assembled following the orientation data. The microscopic model of magneto-elastic behavior of single crystals proposed by Buiron et al. [30] is written using the volumetric fraction f_α of each domain family α (six $\langle 1\,0\,0 \rangle$ families for a cubic symmetry silicon–iron), and magnetization rotation (two angles θ_α and ϕ_α per domain family) as internal variables. The potential energy (5) may be defined for each magnetic domain family f_α as the sum of the magneto-crystalline (6), magnetostatic (7) (magnetic field is considered homogeneous within the grain) and magneto-elastic (8) ($\boldsymbol{\varepsilon}^{\alpha}_{\mu}$: cf. (1)) energies, detailed hereafter.

$$W^{\alpha} = W^{\alpha}_{K} + W^{\alpha}_{H} + W^{\alpha}_{\sigma}, \tag{5}$$

$$W^{\alpha}_{K} = K_1(\gamma_1^2\gamma_2^2 + \gamma_2^2\gamma_3^2 + \gamma_3^2\gamma_1^2) + K_2(\gamma_1^2\gamma_2^2\gamma_3^2), \tag{6}$$

$$W^{\alpha}_{H} = -\mu_0 \vec{H}^{\mathrm{g}} \cdot \vec{M}^{\alpha}, \tag{7}$$

$$W^{\alpha}_{\sigma} = \tfrac{1}{2}\,\boldsymbol{\sigma}^{\alpha} : \mathbb{C}^{\alpha-1} : \boldsymbol{\sigma}^{\alpha} = C^{te} - \boldsymbol{\sigma}^{g} : \boldsymbol{\varepsilon}^{\alpha}_{\mu}, \tag{8}$$

where $\vec{M}^{\alpha} = M_{\mathrm{s}}\vec{\gamma}^{\alpha}$ is the magnetization of the domain family α (M_{s}: saturation magnetization), $\vec{\gamma}^{\alpha}$ denotes the direction of magnetization (γ^{α}_{i}: direction cosines) in CF. K_1 and K_2 are the so-called magnetocrystalline energy constants. $\vec{H}^{\mathrm{g}}$ is the magnetic field at the grain scale. $\boldsymbol{\sigma}^{\alpha}$ and $\boldsymbol{\sigma}^{\mathrm{g}}$ are the stress tensors applied to the domain family and to the grain, respectively. $\mathbb{C}^{\alpha}$ denotes the stiffness tensor of a domain family (or grain). At the grain scale, equilibrium is derived from the combination of an explicit expression based on a Boltzmann function for the

determination of f_α (9) (A_s is an adjusting parameter—see Table 1 and Ref. [18]), and a minimization of the potential energy (5) of a domain family for the determination of θ_α and ϕ_α (10).

$$f_\alpha = \frac{\exp(-A_s.W^\alpha)}{\sum_\alpha \exp(-A_s.W^\alpha)}, \tag{9}$$

$$W^\alpha(\theta_\alpha, \phi_\alpha) = \min(W^\alpha), \quad \theta_\alpha \in [0, \pi], \quad \phi_\alpha \in [0, 2\pi], \tag{10}$$

$$\boldsymbol{\varepsilon}^g_\mu = \langle \boldsymbol{\varepsilon}^\alpha_\mu \rangle = \sum_\alpha f_\alpha \boldsymbol{\varepsilon}^\alpha_\mu, \tag{11}$$

$$\vec{M}^g = \langle \vec{M}^\alpha \rangle = \sum_\alpha f_\alpha \vec{M}^\alpha. \tag{12}$$

Assuming that the elastic behavior is homogeneous within a grain, the magnetostriction strain of a single crystal is written as the mean magnetostriction of each domain (11) ($\langle \cdots \rangle$ denotes an averaging operation). The magnetization in a grain is defined as well (12).

3.2. Localization and homogenization [18]

The previous calculations are made for each grain of the polycrystalline aggregate. The magnetic behavior at polycrystalline scale is defined as the average value of magnetization (13). A local demagnetizing field in each grain due to the magnetization of the surrounding grains is introduced [31,18]: the magnetic field at the grain scale $\vec{H}^g$ is defined as a function of the external field, the mean secant equivalent susceptibility of the material χ_m, ($\chi_m = M/H$) and the difference between the mean magnetization $\vec{M}$ and the magnetization at the grain scale $\vec{M}^g$ (14). The elastic behavior is obtained thanks to a self-consistent homogenization scheme. The macroscopic magnetostriction strain (15) is estimated using Eshelby's solution [32] and considering the local magnetostriction as a free strain; $\mathbb{B}$ denotes the fourth order stress concentration tensor [33,22].

$$\vec{M} = \langle \vec{M}^g \rangle, \tag{13}$$

$$\vec{H}^g = \vec{H} + \frac{1}{3 + 2\chi_m}(\vec{M} - \vec{M}^g). \tag{14}$$

The magnetostriction strain at grain scale is elastically incompatible and creates a stress state affecting the magneto-elastic energy term (self-stress state). The stress at grain scale $\boldsymbol{\sigma}^g$ is derived from the implicit equation (16).

$$\boldsymbol{E}_\mu = \langle {}^t\mathbb{B} : \boldsymbol{\varepsilon}^g_\mu \rangle, \tag{15}$$

$$\boldsymbol{\sigma}^g = \mathbb{B} : \boldsymbol{\Sigma} + \mathbb{C}^{acc} : (\boldsymbol{E}_\mu - \boldsymbol{\varepsilon}^g_\mu) \tag{16}$$

with $\mathbb{C}^{acc} = (\mathbb{C}^g)^{-1} + (\mathbb{C}^0 : ((\mathbb{S}^{Esh})^{-1} - \mathbb{I}))^{-1}$. $\mathbb{C}^0$ being the stiffness tensor of the effective media [33]. Since a self-consistent scheme has been chosen, $\mathbb{C}^0$ refers to the self-consistent stiffness tensor [22]. $\boldsymbol{\Sigma}$ is the macroscopic stress (taken as zero in the present case but denoting the applied stress). $\mathbb{S}^{Esh}$ is the so-called Eshelby's tensor calculated from the Green's functions and ODF [20]. Since this model always refers to equilibrium, modeling results must be compared to anhysteretic experimental measurements.

Figs. 12 and 13 give the results of the multiscale modeling for a magnetization along ⟨1 0 0⟩ and ⟨1 1 0⟩ directions. These directions refer theoretically to RD and TD for the GO material. Results are far from the experimental ones. They are nevertheless in very good accordance with literature concerning 3% Si–Fe single crystals [2]. The reason is that infinite medium hypothesis is made in the multiscale model in its usual form, that makes the behavior corresponding to a single crystal behavior, and not a GO behavior. Infinite medium hypothesis leads to an identical value of the energy of each domain in absence of external loading. The initial volumetric fraction

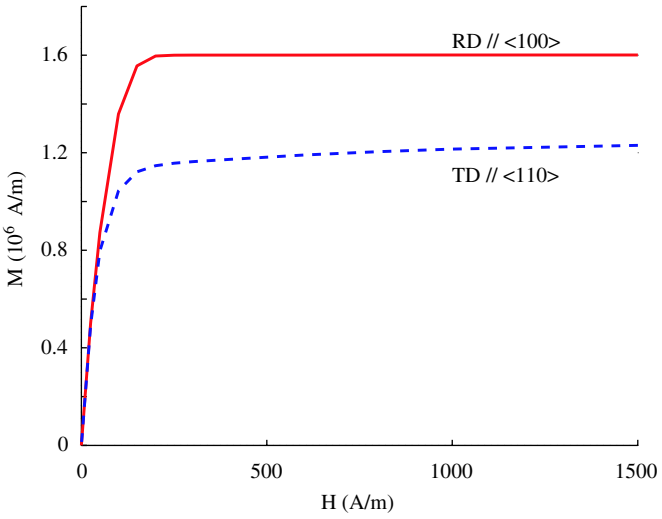

Fig. 12. First result of the multiscale modeling—anhysteretic magnetization curves along ⟨1 0 0⟩ (i.e. RD) and ⟨1 1 0⟩ (i.e. TD).

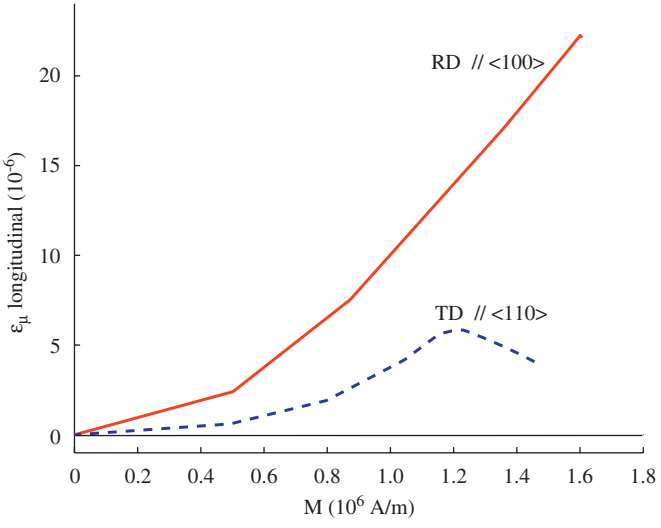

Fig. 13. First result of the multiscale modeling—anhysteretic magnetostriction curves along ⟨1 0 0⟩ (i.e. RD) and ⟨1 1 0⟩ (i.e. TD)—longitudinal magnetostriction.

of each domain family is then identical following Eq. (9) ($\frac{1}{6}$ in the present case). This is not in accordance with the foreseen bi-domains configuration.

3.3. Implementation of a demagnetizing surface effect

The infinite medium hypothesis is not appropriate when the grain size is very high as observed for the sheets studied herein. The model does not take into account that the emerging component of the magnetization is very unfavorable because of the presence of two free surfaces (only a small disorientation is enough to disturb the domain configuration [28,26]). An idea is to take this structural effect into account by adding a specific surface energy term (Eq. (17)) to the potential energy of a domain family (Eq. (5)).

$$W_S^\alpha = N_s(\vec{\gamma}\cdot\vec{z}_0)^2. \tag{17}$$

$\vec{z}_0$ is the direction normal to the sheet and N_s a demagnetizing field factor that defines the maximum level of the surface energy. This energetic term acts as a macroscopic uniaxial anisotropy energy. It is possible to generalize this form to triaxial anisotropy. Factors N_i depend on length, width and thickness of specimen:

$$W_S^\alpha = N_1(\vec{\gamma}\cdot\vec{x}_0)^2 + N_2(\vec{\gamma}\cdot\vec{y}_0)^2 + N_3(\vec{\gamma}\cdot\vec{z}_0)^2. \tag{18}$$

It corresponds to the general form

$$W_S^\alpha = C\vec{\gamma}^t\cdot\mathbb{N}\cdot\vec{\gamma}, \tag{19}$$

where $\mathbb{N}$ is an adimensional anisotropy matrix, and C a constant ($\mathrm{J\,m^{-3}}$). $\mathbb{N}$ exhibits an orthotropic symmetry, related to the parallelepiped geometry of the sample. This anisotropy matrix is therefore diagonal in the sample framework (SaF):

$$\mathbb{N} = \begin{pmatrix} N_{xx} & 0 & 0 \\ 0 & N_{yy} & 0 \\ 0 & 0 & N_{zz} \end{pmatrix}_{\mathrm{SaF}}. \tag{20}$$

Such kind of "form effect" has been yet discussed by many authors [1,2,34]. Each term can nevertheless be analytically calculated if some hypotheses are made about the behavior (supposed most of the time linear), about the surrounding magnetization (supposed most of the time null) and about the shape (supposed most of the time ellipsoidal). It is possible to find in Ref. [35] some guidelines for the evaluation of $\mathbb{N}$. We propose the following linear definition of $\mathbb{N}$ where the grain size $\bar{\phi}_g$ and the characteristic lengths following the three axes appear (L_1, L_2, L_3):

$$\mathbb{N} = \begin{pmatrix} \frac{\bar{\phi}_g}{L_1} & 0 & 0 \\ 0 & \frac{\bar{\phi}_g}{L_2} & 0 \\ 0 & 0 & \frac{\bar{\phi}_g}{L_3} \end{pmatrix}_{\mathrm{SaF}}. \tag{21}$$

On the other hand, it may be possible to link the expression of W_S^α to the usual magnetostatic energy. Surface effect can be seen as the effect of a macroscopic demagnetizing field acting on each domain [10]. The existence of a demagnetizing field at this scale is in disaccordance with the hypothesis of homogeneous magnetic field ($\vec{H}_\alpha = \vec{H}_g$). It is nevertheless possible to define a new localization law from the grain to the domain scale following Eq. (14). We write

$$\vec{H}^\alpha = \vec{H}^g + C_0\mathbb{N}(\vec{M}^g - \vec{M}^\alpha) \approx \vec{H}^g - C_0\mathbb{N}.\vec{M}^\alpha, \tag{22}$$

where C_0 is an adimensional adjusting constant. In this equation, we are considering that the magnetization at grain scale is negligible facing to the magnetization at domain scale. This is a very rough simplification. But it allows us to get an expression where the demagnetizing field at the domain scale is constant:

$$\vec{H}_d^\alpha = -C_0\mathbb{N}.\vec{M}^\alpha. \tag{23}$$

The new definition of the local magnetic field leads to a new definition of the magnetostatic energy:

$$\begin{aligned} W_H^{\alpha'} &= -\mu_0\vec{H}^\alpha.\vec{M}^\alpha = -\mu_0\vec{H}^g.\vec{M}^\alpha + \mu_0 C_0(\mathbb{N}.\vec{M}^\alpha).\vec{M}^\alpha \\ &= W_H^\alpha + W_S^\alpha. \end{aligned} \tag{24}$$

The demagnetizing surface energy appears as a part of the potential energy. The constant C in Eq. (19) is now corresponding to $C = \mu_0 C_0 M^{\alpha 2} \approx \mu_0 C_0 M_s^2$. Finally, we define

$$W_S^\alpha = \mu_0 C_0 M_s^2\vec{\gamma}^t.\mathbb{N}.\vec{\gamma}. \tag{25}$$

The numerical applications[10] give $N_{xx} \approx 0$, $N_{yy} = 3$ and $N_{zz} = 150$. C_0 is the only additional parameter, to be identified thanks to experimental data (M_s is given in Table 1). We find $C_0 = 8.19 \times 10^{-7}$ and so $N_s \approx 400\,\mathrm{J\,m^{-3}}$ in the simplified expression (17).

4. Results of the model and comparison to experimental data

Table 1 gives the different physical and numerical constants used to model the GO laminations behavior. Fig. 14 shows a good agreement between the magnetization predictions and experimental data. The influence of the demagnetizing surface effect is clearly highlighted, especially concerning the initial susceptibility. Figs. 15 and 16 show the different results of the model for magnetostriction. Magnetostriction is very sensitive to the surface effect: a complete inversion of RD and TD previsions is observed compared to the infinite medium conditions (Fig. 13). The modeling seems particularly accurate for the longitudinal behavior. The higher difference is for the transversal measurement of the TD sample. We observe that the modeled magnetostriction is saturating at -32×10^{-6}, compared to -37×10^{-6} for the experiment. Nevertheless this experimental result exceeds the saturation bound

[10] The characteristic length L_1 can be considered as infinite because the specimen is considered *inside* the experimental set-up.

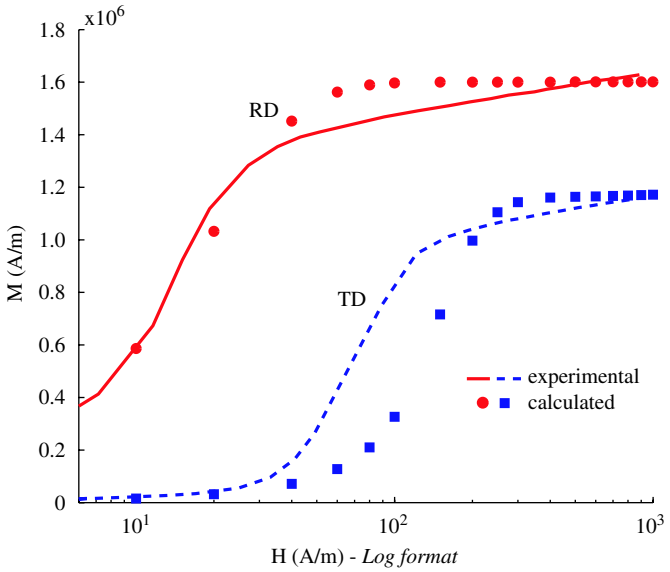

Fig. 14. Comparison between experimental (lines) and modeled (points) anhysteretic magnetization curves along RD and TD.

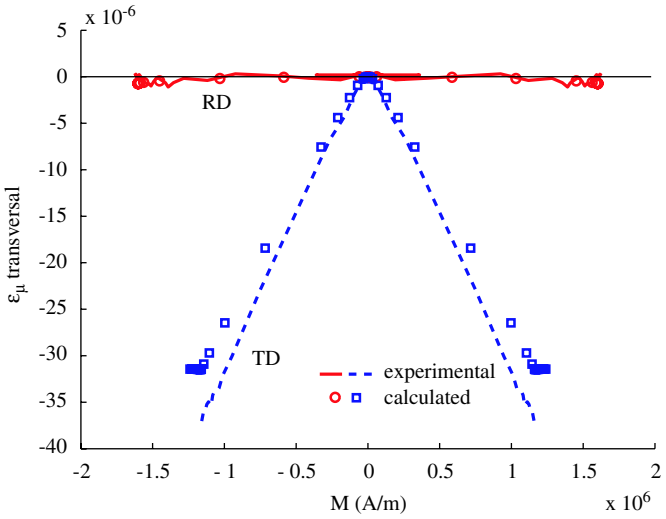

Fig. 16. Comparison between experimental (lines) and modeled (points) anhysteretic magnetostriction curves along RD and TD—transversal measurements.

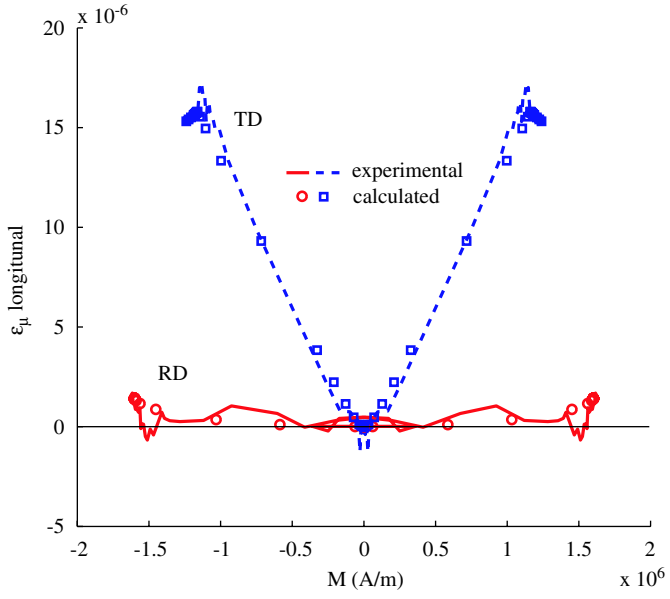

Fig. 15. Comparison between experimental (lines) and modeled (points) anhysteretic magnetostriction curves along RD and TD—longitudinal measurements.

defined in paragraph 2.3 (i.e. -34.5×10^{-6}). That observation seems to prove that the magnetostrictive constants we used, and especially λ_{100} may be under-estimated. It could be due to a short difference in composition between the GO used for the experiments and the 3% silicon–iron of the literature.

The strong change of magnetostriction behavior is due to a complete re-organization of the domains at zero external magnetic field. The volumetric fraction of all domain families is $\frac{1}{6}$ without surface effect. An introduction of the demagnetizing term creates differences between the energy of the domain families in a grain. In the present case the volumetric fraction of the domains oriented along RD increases reaching about 70–90% because of their lowest energy. This heterogeneous distribution is in accordance with experimental observations (Fig. 17[11] and see [28]). Magnetostriction along RD is close to the saturation at the beginning of magnetization. The amplitude of the magnetostriction is consequently very small in this direction.

5. Conclusion

Modeling and experimental results of the magnetic and magnetostrictive behavior of a grain-oriented (GO) silicon steel have been presented in this paper. The experiments consisted mainly in anhysteretic magnetization and magnetostriction measurements, which have been successfully compared to results from the literature. A multiscale model, based on an energetic approach and infinite medium hypothesis, has been used in a first modeling. Significant discrepancies between experiments and predictions have been highlighted, due to the influence of free surfaces combined to the large grain size, not taken into account. It is shown that the introduction of a structural demagnetizing term in the multiscale model allows an appropriate correction of the predictions of the magnetic and magnetostrictive behavior.

We are now able to describe the difference of magneto-mechanical behavior between a GO lamination and a single crystal magnetized along the same crystallographic direction. Such a structural effect could on the other hand explain why measurements of magnetostriction of GO laminations lead sometimes to very variable results.

[11]Observations made in association with S. Courtois and E. Hug from the UTC-Compiègne (France).

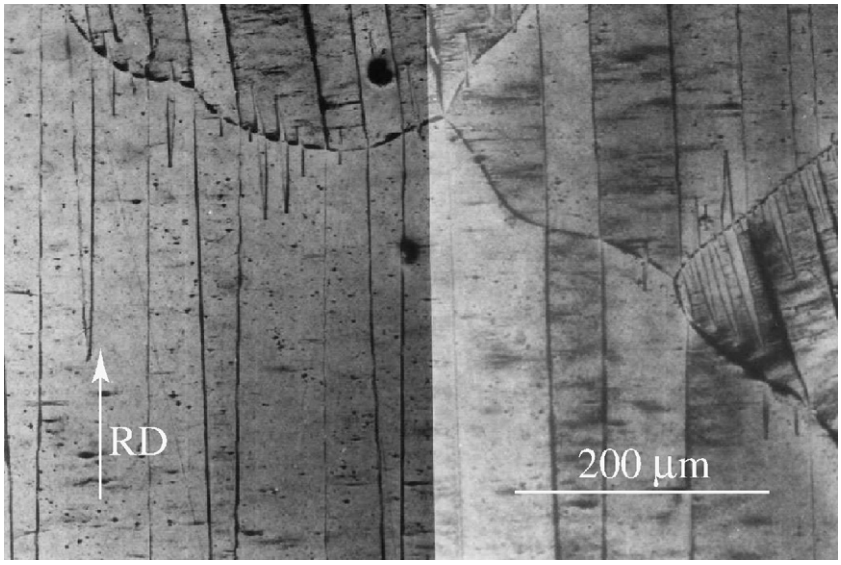

Fig. 17. Optical observation of the magnetic domains—dominant type I structure aligned along RD—Bitter technique.

This work highlights finally that the magnetic structure is not unique for a given magnetization. The improved multiscale model does nevertheless not give a topological description of domains (i.e. lancets, or closure domains), but only volumetric fractions of domain families. Improvements will consist in taking into account the interaction between the domains of a same grain and the neighboring grains (interaction clearly illustrated in Fig. 17).

However, in its present form, the multiscale model allows us to model the influence of an applied stress on the magneto-elastic behavior. An implementation in a finite element calculation is now possible in order to evaluate the magneto-elastic response of a complex magnetic circuit made of stacked GO sheets.

References

[1] R.M. Bozorth, Ferromagnetism, Van Norstand Company, Berlin, New York, 1951.
[2] B.D. Cullity, Introduction to Magnetic Materials, Addison-Wesley, Reading MA, 1972.
[3] J.W. Shilling, G.L. Houze Jr., IEEE Trans. Magn. 10 (2) (1974) 195.
[4] W.M. Swift, J.W. Shilling, S.K. Bhate, F.J. Young, IEEE Trans. Magn. 10 (5) (1974) 810.
[5] F. Fiorillo, C. Appino, C. Beatrice, F. Garsia, J. Magn. Magn. Mater. 242–245 (2002) 257.
[6] A. Böttcher, T. Gerber, K. Lücke, Mater. Sci. Tech. 8 (1992) 16.
[7] H. Masui, IEEE Trans. Magn. 31 (2) (1995) 930.
[8] E. Hug, J. Mater. Sci. 30 (1995) 4417.
[9] G. Ban, F. Janosi, J. Magn. Magn. Mater. 160 (1996) 167.
[10] P.T. Squire, S.N. Hogsdon, H. Hauser, J. Magn. Magn. Mater. 157–158 (1996) 527.
[11] C. Krell, N. Baumgartinger, G. Krismanic, E. Leiss, H. Pfützner, J. Magn. Magn. Mater. 215–216 (2000) 634.
[12] L. Hirsinger, L. Billardon, J. Magn. Magn. Mater. 140 (2002) 2199.
[13] B. Weiser, H. Pfützner, IEEE Trans. Magn. 36 (5) (2000) 3759.
[14] O. Hubert, L. Daniel, R. Billardon, J. Magn. Magn. Mater. 254–255C (2003) 352.
[15] Z. Ren, A. Razek, IEEE Trans. Magn. 28 (2) (1992) 1212.
[16] L. Vandevelde, J.A.A. Melkebeek, IEEE Trans. Magn. 38 (2) (2002) 993.
[17] E. Du Trémolet de Lacheisserie, Magnetism—Fundamentals, Materials and Applications, Springer, Berlin, 2002.
[18] L. Daniel, O. Hubert, N. Buiron, R. Billardon, J. Mech. Phys. Solids 56 (3) (2008) 1018.
[19] C. Buvat, Ph.D. Thesis, University Paris 6, 2000.
[20] L. Daniel, Ph.D. Thesis, ENS-Cachan, September 2003.
[21] D. Francois, A. Pineau et Zaoui, Mechanical Behaviour of Materials, Vol. I: Elasticity and Plasticity, Kluwer Academic Publisher, Dordrecht, 1998.
[22] L. Daniel, O. Hubert, F. Ossart, R. Billardon, J. Phys. IV 105 (2003) 247.
[23] C. Gourdin, Ph.D. Thesis, University Paris 6, 1997.
[24] A.C. Eringen, G.A. Maugin, Electrodynamics of Continua—I: Foundations and Solid Media, Springer, Berlin, 1990.
[25] N. Galopin, et al., Rev. Int. Génie Electrique 9 (4–5) (2006) 499.
[26] Y. Ushigami, M. Mizokami, M. Fujikura, T. Kubota, H. Fujii, K. Murakami, J. Magn. Magn. Mater. 254–255 (2003) 307.
[27] L. Sheiko, A. Moroshkin, S. Gaiduk, J. Magn. Magn. Mater. 157–158 (1996) 457.
[28] A. Hubert, R. Schäfer, Magnetic Domains, Springer, Berlin, 1998.
[29] W.J. Carr, in: A.E. Berkowitz, E. Kneller (Eds.), Magnetism and Metallurgy, Academic Press, New York, 1969, p. 45.
[30] N. Buiron, L. Hirsinger, R. Billardon, J. Phys. IV 11 (2001) 373.
[31] L. Daniel, O. Hubert, R. Billardon, Comp. Appl. Math. 23 (2–3) (2004) 285.
[32] J.D. Eshelby, Proc. R. Soc. Lond. A 421 (1957) 376.
[33] R. Hill, J. Mech. Phys. Solids 13 (1965) 213.
[34] S. Chikazumi, Physics of Ferromagnetism, second ed., Oxford University Press, 1997.
[35] R. Gersdorf, Physica 26 (1960) 553.